Monthly Notices
of the
ROYAL ASTRONOMICAL SOCIETY

MNRAS **472,** 713–726 (2017)
Advance Access publication 2017 August 4

doi:10.1093/mnras/stx1999

Excess entropy and energy feedback from within cluster cores up to r_{200}

Asif Iqbal,[1⋆] Subhabrata Majumdar,[2⋆] Biman B. Nath,[3] Stefano Ettori,[4,5] Dominique Eckert[6] and Manzoor A. Malik[1⋆]

[1]*Department of Physics, University of Kashmir, Hazratbal, Srinagar, J&K 190011, India*
[2]*Tata Institute of Fundamental Research, 1 Homi Bhabha Road, Mumbai 400005, India*
[3]*Raman Research Institute, Sadashiva Nagar, Bangalore 560080, India*
[4]*INAF, Osservatorio Astronomico di Bologna, Via Ranzani 1, I-40127 Bologna, Italy*
[5]*INFN, Sezione di Bologna, viale Berti Pichat 6/2, I-40127 Bologna, Italy*
[6]*Astronomy Department, University of Geneva 16, ch. d'Ecogia, CH-1290 Versoix, Switzerland*

Accepted 2017 August 2. Received 2017 July 11; in original form 2017 February 28

ABSTRACT

We estimate the 'non-gravitational' entropy-injection profiles, ΔK, and the resultant energy feedback profiles, ΔE, of the intracluster medium for 17 clusters using their *Planck* Sunyaev–Zel'dovich and *ROSAT* X-ray observations, spanning a large radial range from $0.2r_{500}$ up to r_{200}. The feedback profiles are estimated by comparing the observed entropy, at fixed gas mass shells, with theoretical entropy profiles predicted from non-radiative hydrodynamic simulations. We include non-thermal pressure and gas clumping in our analysis. The inclusion of non-thermal pressure and clumping results in changing the estimates for r_{500} and r_{200} by 10–20 per cent. When clumpiness is not considered it leads to an underestimation of $\Delta K \approx 300\,\mathrm{keV\,cm^2}$ at r_{500} and $\Delta K \approx 1100\,\mathrm{keV\,cm^2}$ at r_{200}. On the other hand, neglecting non-thermal pressure results in an overestimation of $\Delta K \approx 100\,\mathrm{keV\,cm^2}$ at r_{500} and underestimation of $\Delta K \approx 450\,\mathrm{keV\,cm^2}$ at r_{200}. For the estimated feedback energy, we find that ignoring clumping leads to an underestimation of energy per particle $\Delta E \approx 1\,\mathrm{keV}$ at r_{500} and $\Delta E \approx 1.5\,\mathrm{keV}$ at r_{200}. Similarly, neglect of the non-thermal pressure results in an overestimation of $\Delta E \approx 0.5\,\mathrm{keV}$ at r_{500} and underestimation of $\Delta E \approx 0.25\,\mathrm{keV}$ at r_{200}. We find entropy floor of $\Delta K \approx 300\,\mathrm{keV\,cm^2}$ is ruled out at $\approx 3\sigma$ throughout the entire radial range and $\Delta E \approx 1\,\mathrm{keV}$ at more than 3σ beyond r_{500}, strongly constraining intracluster medium pre-heating scenarios. We also demonstrate robustness of results w.r.t. sample selection, X-ray analysis procedures, entropy modelling, etc.

Key words: galaxies: clusters: intracluster medium – cosmological parameters.

1 INTRODUCTION

Clusters of galaxies are the largest evolved structures in the universe and, as such, qualify for being important cosmological probes. The abundance of galaxy clusters provides sensitive constraints on the cosmological parameters that govern the growth of structures in the universe (Holder et al. 2001; Gladders et al. 2007; Vikhlinin et al. 2009). In this regard, X-ray observations provide a useful tool for identifying and studying galaxy clusters (Birzan et al. 2004; Pratt et al. 2010; Eckert et al. 2013a,b). Galaxy clusters can also be observed in the microwave band through Sunyaev–Zel'dovich (SZ) effect (Sunyaev & Zeldovich 1972, 1980), which results from the up-scatting of cosmic microwave background photons by hot electrons in the intracluster medium (ICM). The SZ effect has a unique property that unlike X-ray emission it is independent of redshift and does not suffer from cosmological dimming. With the current and upcoming data from *Planck*, the SZ cluster surveys have become a robust probe for determining cosmological parameters and global properties of ICM (Eckert et al. 2013a; Planck Collaboration V 2013b; McCarthy et al. 2014; Planck Collaboration XX 2014; Ettori 2015).

However, in order to obtain robust cosmological estimates using such techniques one requires the precise knowledge of the evolution of galaxy clusters with redshift and the thermodynamical properties of ICM. In the simplest case, where one considers a pure gravitational collapse, the cluster scaling relations are expected to follow simple self-similarity (Kaiser 1986). Correlations between the X-ray properties are widely used to probe the self-similarity in the galaxy clusters. For example, the luminosity–temperature (L_x–T) relation for self-similar models predicts a shallower slope ($L_x \propto T^2$) than observed ($L_x \propto T^3$) (Edge & Stewart 1991; Markevitch 1998) implying a break in the self-similarity in galaxy clusters.

⋆ E-mail: asifiqbal@kashmiruniversity.net (AI); subha@tifr.res.in (SM); mmalik@kashmiruniversity.ac.in (MAM)

Similarly, studies of the scaling relations involving SZ effect also show discrepancies between observations and predictions from a pure gravitational model (Holder & Carlstrom 2001; Battaglia 2012). Such studies have revealed the importance of the complex non-gravitational processes, such as injection of energy feedback from active galactic nuclei, radiative cooling, supernovae and star formation, influencing the thermal structure of ICM, particularly in low-mass (temperature) clusters (Roychowdhury et al. 2005; Voit et al. 2005; Chaudhuri et al. 2012, 2013).

The first direct evidence for non-gravitational entropy in galaxy clusters and galaxy groups was given by David et al. (1996) using *ROSAT* Position Sensitive Proportional Counter (PSPC) observations. The observations showed that there was excess entropy compared to that expected from gas collapsing in a gravitational potential. Motivated by these findings, several groups have drawn similar conclusions using both numerical and semi-analytical models with an entropy floor of the order of 300–400 keV cm^2 (Ponman et al. 1999; Tozzi & Norman 2001; Chaudhuri et al. 2012, 2013; Eckert et al. 2013a). Although, SNe feedback are essential to explain the enrichment of the ICM to the observed metallicity level and heavy-element abundances, they provide insufficient amount of energy per particle as compared to recent observations. Moreover, they are also inefficient to quench cooling in massive galaxies (Springel et al. 2005). There is a growing evidence that active galactic nucleus (AGN) feedback mechanism provides a major source of heating for the ICM gas, thereby reducing number of cooling flow clusters (McNamara & Nulsen 2007; Gaspari et al. 2011; Chaudhuri et al. 2012, 2013; Gaspari et al. 2014). The AGN-jet simulations show that such mechanisms can overcome the cooling flow over a cosmological time-scale and produce results similar to observations (Gaspari et al. 2012, 2014; Li et al. 2015).

Moreover, it has been found with Suzaku observations that the entropy profile flattens out at large radii (Hoshino et al. 2010; Simionescu et al. 2011; Eckert et al. 2013a; Fujita et al. 2013). This entropy decrement can be related to the gas clumping (Simionescu et al. 2011; Eckert et al. 2013a, 2015), presence of non-thermal pressure (Fusco-Femiano & Lapi 2014; Su et al. 2015), accretion/merger shocks in outskirts of clusters (Hoshino et al. 2010; Cavaliere et al. 2011), loss of kinetic energy of gas due to the cosmic ray acceleration (Fujita et al. 2013; Su et al. 2015) or due to the rapid temperature decrease in the outskirts of clusters as a result of the non-gravitational processes (Fusco-Femiano & Lapi 2014).

It is convenient to define an entropy profile[1] of gas as, $K_g(r) = kTn_e(r)^{-2/3} \propto P(r)\rho(r)^{-\gamma}$, where k is the Boltzmann constant, and the exponent $\gamma = 5/3$ refers to the adiabatic index. With this definition, K_g remains unchanged for all adiabatic processes and can therefore probe the thermal history of gas. Purely gravitational models predict entropy profiles in clusters of the form $K_g(r) \propto r^{1.1}$ (Voit et al. 2005). However, as pointed, several recent observations found deviations from this expected entropy profile, especially at inner and outer radii (Voit et al. 2005; Cavagnolo et al. 2009; Pratt et al. 2010; Eckert et al. 2013a) as a result of non-gravitational feedback. To allow a meaningful interpretation and to estimate degree of feedback, one needs to compare recent observations with theoretically expected profiles with no feedback.

Previously, Chaudhuri et al. (2012, 2013) estimated the non-gravitational energy deposition profile up to r_{500} by comparing the observed entropy profiles with a benchmark entropy profile without feedback (Voit et al. 2005) for the REXCESS sample of 31 clusters (Pratt et al. 2010) observed with *XMM–Newton*. They found an excess mean energy per particle of 2.74 and 1.64 keV using benchmark entropy from adaptive mesh refinement (AMR) and smoothed particle hydrodynamics (SPH) simulations respectively, along with a strong correlation for AGN feedback. Our study extends their work by going beyond r_{500}. Here, we consider the joint data set of *Planck* SZ pressure profile and *ROSAT* gas density profiles of 17 clusters (Eckert et al. 2013a,b; Planck Collaboration V 2013b) to estimate the excess entropy and feedback energy profiles up to r_{200}. Recent simulations show significant level of non-thermal pressure from bulk motion (Rasia et al. 2004; Battaglia 2012; Shi et al. 2015) and gas clumping (which by definition is measured by $C = \langle\rho_g^2\rangle/\langle\rho_g\rangle^2$) (Nagai et al. 2011; Eckert et al. 2013a, 2015; Battaglia et al. 2015) in the outer regions of ICM. We, therefore, incorporate both these factors in our calculations.

This paper is a continuation of our recent work Iqbal et al. (2017) wherein we showed that pre-heating scenarios are ruled out at more than 3σ statistical level. In this work, we present a detailed study of the excess entropy profiles along with feedback energy profiles and discuss the effect of non-thermal pressure and clumping in our estimates. We also look at sample selection, cool-core versus non-cool-core clusters, effects of boundary conditions, choice of benchmark theoretical entropy profiles, choice of X-ray methodology, etc.

The paper is organized as follows: In Section 2, we describe the cluster sample used in this work. In Section 3, we describe the self-similar non-radiative model for galaxy clusters. Section 4 is dedicated to the determination of excess entropy and energy profiles, and the effects of the non-thermal pressure and gas clumping on their estimates. In Section 5, we check the robustness of our results. In Section 6, we compare the feedback profiles for AMR and SPH benchmark entropy profiles. Section 7 gives the comparison of our results with the previous estimates. Finally, the conclusions of our work is given in last section. Throughout this paper, we assume cosmology where $(\Omega_m, \Omega_\Lambda, H_0) = (0.3, 0.7, 70)$.

2 CLUSTER SAMPLE AND DATA SET

In this work, we have studied a sample of 17 clusters in the redshift range (0.04–0.2) that are common in Planck Collaboration V (2013b) and Eckert et al. (2012). Based on their central entropy (Cavagnolo et al. 2009), six of these clusters are classified as cool-core ($K_0 < 30$ keV cm^2), while the remaining 11 are non-cool core.

This sample was earlier used by Eckert et al. (2013a,b)[2] where they have shown that the thermodynamic state of the ICM can be accurately recovered by using the *Planck* SZ pressure profile (Planck Collaboration V 2013b) and *ROSAT* PSPC gas density profile (Eckert et al. 2012).[3] Since the SZ signal is proportional to the integrated pressure (gas density), unlike the X-ray signal, which is proportional to the square of density, it decreases more gently at large radius and therefore can provide more accurate pressure profiles in the cluster outskirts. This allows us to accurately recover the temperature profile beyond r_{500}. We use parametric profiles

[1] Thermodynamic definition of specific entropy being $S = \ln K_g^{3/2} +$ constant.

[2] www.isdc.unige.ch/~deckert/newsite/Dominique_Eckerts_Homepage.html

[3] The cluster 'A2163' from Eckert et al. (2013a,b) sample has been left out as its estimated feedback profile was found hugely different from others. This cluster has been found to be in a perturbed state (Soucail 2012).

obtained by them in this work (see Eckert et al. 2013a for more details) which were obtained by fitting a functional form to the projected emission-measure data (Vikhlinin et al. 2006) and *Planck* SZ pressure data (Nagai et al. 2007). The errors were obtained through Monte Carlo Markov Chain, with direct sampling of the posterior temperature, entropy and gas fraction distributions.

Eckert et al. (2013a) also obtained deprojected profiles by estimating density profile through 'onion peeling' technique (Kriss et al. 1983; Eckert et al. 2012) and interpolating the SZ pressure profile. Correction for edge effects were also applied along with median smoothing regularization for minimizing the roller-coaster effect (McLaughlin 1999). The error bars were recovered by perturbing the original profile using a Monte Carlo and recomputing the deprojected profiles each time.

Since the parametric profiles are forced to be regular, this reduces the cluster to cluster scatter and the errors. At smaller radii the angular resolution of both *Planck* and *ROSAT* is insufficient to obtain reliable constraints. Therefore, the parametric fitting was only performed on the data beyond $0.2r_{500}$ and were found to be consistent with the deprojected profiles.

3 THEORETICAL MODELS

3.1 Cluster model

We use the hydrostatic equation to obtain the total mass profile $M_{\rm tot}(r)$ in the galaxy clusters

$$M_{\rm tot}(r) \;=\; -\frac{r^2}{G\rho_{\rm g}(r)}\,\frac{{\rm d}P_{\rm g}(r)}{{\rm d}r}, \qquad (1)$$

where $\rho_{\rm g}$ and $P_{\rm g}$ are density and thermal pressure of the ICM, respectively. ${\rm d}P_{\rm g}(r)/{\rm d}r$ is calculated by using the best-fitting generalized NFW (GNFW) pressure profile (Planck Collaboration V 2013b). The quantities r_{500} and r_{200} where obtained by first interpolating the $M_{\rm tot}(r)$ profile and then iteratively solving[4]

$$m_{\Delta} \;=\; 4/3\; r_{\Delta}^3\; \Delta\; \rho_{\rm c}(z). \qquad (2)$$

The virial radius, $r_{\rm vir}(m_{\rm vir},\, z)$, is calculated with the help of the spherical collapse model (Bryan & Norman 1998). If required, the mass profile is obtained by linear extrapolation in logarithmic space.

Recent simulations suggest that a significant non-thermal pressure contributes to the total energy of the ICM gas, mainly due to bulk gas motions and turbulence in the ICM gas (Vazza et al. 2009; Battaglia 2012; Shi et al. 2015). While non-thermal pressure is small in the inner region, its relative importance steadily increases with radius, becoming a significant fraction of the total pressure in the outer region (Lau et al. 2009). It has been found from both observations and simulations that m_{500} is underestimated by about 10–20 per cent, if one uses the hydrostatic equation without non-thermal pressure (Rasia et al. 2004; Shi et al. 2015). From the recent numerical simulations, we model the non-thermal pressure fraction in the power-law form similar to that given in Shaw et al. (2010)

$$P_{\rm nt}(r,z) \;=\; f(r,z)\; P_{\rm tot} \;=\; \frac{f(r,z)}{1-f(r,z)}\; P_{\rm g}(r), \qquad (3)$$

where $P_{\rm tot}$ is the total gas pressure, $f(r,z) = a(z)(\frac{r}{r_{500}})^{n_{\rm nt}}$, $a(z) \;=\; a_0(1\,+\,z)^{\beta}$ for low-redshift clusters ($z \,\leq\, 1$) with

[4] Δ is defined such that r_{Δ} is the radius out to which mean matter density is $\Delta\rho_{\rm c}$, where $\rho_{\rm c} = 3H^2(z)/8\pi G$ being critical density of the universe at redshift z.

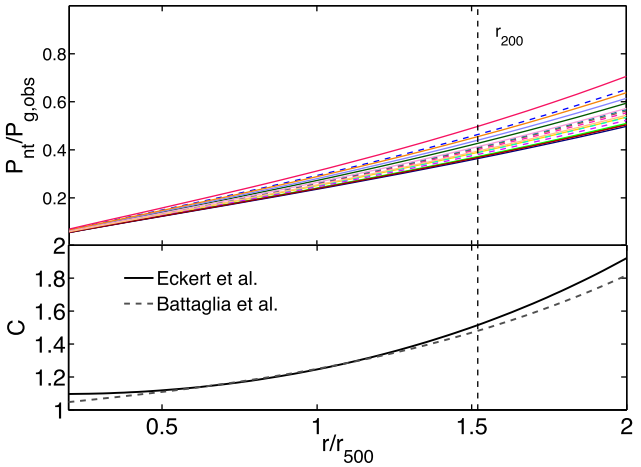

Figure 1. Upper panel: Variation of $P_{\rm nt}/P_{\rm g}$ as a function r/r_{500} for all the clusters. $P_{\rm g}$ is obtained by using the best-fitting GNFW pressure profile from Planck Collaboration V (2013b). Solid lines represent NCC clusters and dashed lines represent CC clusters. Lower panel: Comparison between Eckert et al. (2015) and Battaglia et al. (2015) clumping profiles for the average case.

$a_0 = 0.18 \pm 0.06$, $\beta = 0.5$ and $n_{\rm nt} = 0.8 \pm 0.25$ (Shaw et al. 2010). In upper panel of Fig. 1 , we have plotted $P_{\rm nt}/P_{\rm g}$ as a function r/r_{500}. It can be seen that $P_{\rm nt}$ becomes $\sim$50 per cent of the thermal gas pressure $P_{\rm g}$ in the cluster outskirts. Since non-thermal pressure is not negligible beyond r_{500}, one should take it into account in order to properly study the cluster physics in the outer regions.

Similarly, it has been seen that gas clumping results in an overestimation of the observed gas density ($\rho_{\rm g,obs}$) and hence underestimation of the entropy and total mass profiles. It has been found from various observations and hydrodynamical simulations that the clumping factor is negligible in the innermost cluster regions but radially increases with $\sqrt{C} \approx 1{-}2$ around r_{200} (Mathiesen 1999; Nagai et al. 2011; Vazza et al. 2013; Battaglia et al. 2015). However, few works have also reported either smaller or higher values of clumping factor (Fusco-Femiano & Lapi 2013; Walker et al. 2013; Fusco-Femiano & Lapi 2014; Urban et al. 2014). Eckert et al. (2015) found that the azimuthal median is a good tracer of the true 3D density ($\rho_{\rm g,true}$) and showed from both hydrodynamical simulations that their method recovered the $\rho_{\rm g,true}$ profiles with deviations less than 10 per cent at all radii. They recovered the average $\sqrt{C} = 1.25$ at r_{200}, which is consistent with the recent results. Lower panel of Fig. 1 shows the consistency of Eckert et al. (2015) clumping profile with that of Battaglia et al. (2015).

We have also calculated the total mass profile $M_{\rm tot}$ by including non-thermal pressure $P_{\rm nt}$ in equation (1) and correcting the density profile using Eckert et al. (2015) clumping profile. In Table 1, we give estimates of r_{500} and r_{200} obtained by using parametric density profiles along with *Planck* best-fitting GNFW pressure profile (Planck Collaboration V 2013b). For comparison, we have also given *Planck* r_{500} values from Planck Collaboration XI (2011) which are consistent with our estimates within 10 per cent for most of the clusters. Moreover, we find that the average scaling $r_{200} = 1.52r_{500}$ (Pointecouteau et al. 2005; Arnaud et al. 2010; Eckert et al. 2013a) is in excellent agreement with our results with small scatter.

Table 1. Values of r_{500} and r_{200} in kpc.

				$P_{nt} = 0$		$P_{nt} \neq 0$	
Cluster	z	State	r_{500}^{planck}	r_{500}	r_{200}	r_{500}	r_{200}
A85	0.052	CC	1206	1300 (105)	2319 (72)	1422 (147)	2390 (51)
A119	0.044	NCC	1114	1026 (49)	2070 (113)	1101 (64)	2188 (46)
A401	0.075	NCC	1355	1265 (53)	1883 (140)	1340 (61)	2038 (182)
A478	0.088	CC	1326	1309 (56)	1923 (153)	1390 (65)	2100 (214)
A665	0.182	NCC	1331	1162 (56)	1846 (123)	1262 (69)	2036 (144)
A1651	0.084	NCC	1135	1165 (62)	1946 (250)	1247 (81)	2186 (61)
A1689	0.183	NCC	1339	1368 (54)	1877 (103)	1449 (60)	2010 (125)
A1795	0.062	CC	1254	1246 (58)	1864 (151)	1337 (69)	2058 (202)
A2029	0.078	CC	1392	1332 (58)	1989 (154)	1421 (68)	2182 (207)
A2204	0.152	CC	1345	1307 (52)	1877 (124)	1388 (60)	2035 (161)
A2218	0.171	NCC	1151	1001 (35)	1496 (105)	1058 (43)	1624 (139)
A2255	0.081	NCC	1169	1252 (73)	1827 (122)	1352 (82)	1971 (143)
A2256	0.058	NCC	1265	1314 (50)	1781 (95)	1390 (56)	1905 (116)
A3112	0.070	CC	1062	1015 (40)	1459 (97)	1076 (45)	1586 (132)
A3158	0.060	NCC	1124	1037 (43)	1521 (100)	1105 (48)	1656 (133)
A3266	0.059	NCC	1354	1478 (121)	2592 (85)	1652 (166)	2683 (35)
A3558	0.047	NCC	1170	1126 (64)	2017 (252)	1217 (83)	2269 (49)

Columns (1), (2), (3) and (4) shows cluster names, redshift, state and r_{500} values from Planck Collaboration XI (2011), respectively. Columns (5) and (6) shows values r_{500} and r_{200} for $P_{nt} = 0$ case. Columns (7) and (8) shows values of r_{500}, r_{200} for $P_{nt} \neq 0$ case.
The numbers in brackets indicate increase in r_{500} and r_{200} if clumping is taken into account.

3.2 Initial entropy profile

Standard models of large-scale structure show that matter is shock heated as it falls into clusters under the influence of gravity and predict that the entropy of gas ($K_{g,th}$) should behave as a power law, with entropy profiles flattening near cluster cores. Voit et al. (2005) performed several non-radiative SPH and AMR simulations in order to study the main features of the entropy profiles. They found differences in entropy profiles in the inner cores but the differences were small for $r > 0.2r_{200}$ in SPH and AMR simulations. They found that the simulated non-radiative scaled entropy profile can be described by a simple power law form in the range $(0.2–1)r_{200}$ with a slightly higher normalization for AMR case. For the inner radii, Voit et al. (2005) found a large discrepancy in the scaled entropy profiles between the SPH and AMR simulations. A flat entropy core has been observed in the centre of non-radiative galaxy clusters in Eulerian grid codes (AMR) which is absent in Lagrangian approaches (SPH). However, after accounting for certain hydrodynamical processes (i.e. shocks and mixing motions) the results of SPH simulations match with that of AMR case (Mitchell et al. 2009; Vazza et al. 2011; Power et al. 2014). We use AMR and SPH median entropy profiles obtained by Voit et al. (2005) for our baseline model described by

$$\frac{K_{g,th}}{K_{200}} = a_0 \left(\frac{r}{r_{200}}\right)^{1.1}, \tag{4}$$

in the range $(0.2–1)r_{200}$ plus by a flatter core below $0.2r_{200}$ which is much more pronounced in case of AMR simulations. a_0 is equal to 1.32 and 1.41 for SPH and AMR respectively and K_{200} is given by

$$K_{200} = 144 \left(\frac{m_{200}}{10^{14}\mathrm{M}_\odot}\right)^{2/3} \left(\frac{1}{f_b}\right)^{2/3} h(z)^{-2/3}\ \mathrm{keV\ cm^2}, \tag{5}$$

where f_b is the universal baryonic fraction and $h(z) = H(z)/H_0$, $H(z)$ being Hubble constant at redshift z.

In order to calculate the initial (without feedback) density (or gas mass) and temperature profiles, one solves the hydrostatic equation with appropriate boundary condition (Chaudhuri et al. 2012, 2013). Considering non-thermal pressure component, we rewrite the hydrostatic equation as

$$\frac{\mathrm{d}(P_{g,th} + P_{nt,th})}{\mathrm{d}r} = -\left(\frac{P_{g,th}}{K_{g,th}}\right)^{3/5} m_p \mu_e^{2/5} \mu^{3/5} \frac{GM_{tot}(<r)}{r^2}, \tag{6}$$

where $P_{g,th} = n_{g,th} k T_{th}$ is the initial (theoretical) thermal pressure of the ICM, T_{th} is the initial ICM temperature and M_{tot} is the sum of two terms, $M_{tot} = M_{thermal} + M_{non\text{-}thermal}$. Since energy injection only effects the gas mass profile, one can assume the dark matter profile and hence total mass profile to remain constant during the feedback processes. For the boundary condition we assume the gas fraction ($f_{g,th}$) to be $0.9f_b$ at virial radius (Crain et al. 2007). On the addition of non-thermal pressure, the initial entropy profile is increased due to the overall increase in the normalization and therefore, the deviation from the observed entropy decreases.

It is important to note that initial entropy profile also depends on the baryonic fraction through K_{200}. Most of the previous estimates of the entropy floor were based on the *WMAP*7 estimates of $f_b = 0.167$ and since the *Planck* predicts relatively lower value of $f_b = 0.156$ (Planck Collaboration III 2013a; Planck Collaboration XIII 2015), this will further increase the initial entropy profile thereby decreasing the estimates of excess entropy.

3.3 Estimates of total feedback energy

In this section, we estimate the total mechanical feedback energy. It is important to note that for a meaningful interpretation, one should compare the theoretical and observed entropy profiles at the same gas mass (m_g) instead of same radii in order to provide an allowance for redistribution of gas on account of feedback processes (Li et al. 2011; Nath & Majumdar 2011; Chaudhuri et al. 2012, 2013). Considering a transformation from the baseline configuration to new configuration i.e. $\Delta K(m_g) = K_{g,obs}(m_g) - K_{g,th}(m_g)$, the additional thermal energy per particle in ICM corresponding to the

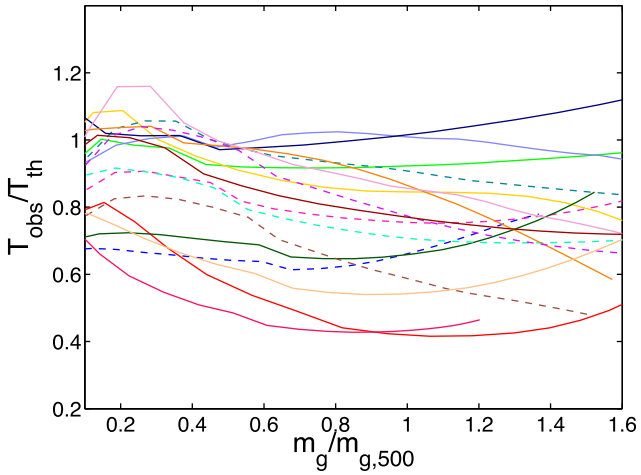

Figure 2. This plot shows variation of $T_{\rm obs}/T_{\rm th}$ as a function $m_{\rm g}/m_{\rm g,\,500}$ for all the clusters (considering clumping and $P_{\rm nt} \neq 0$). Solid lines represent NCC clusters and dashed lines represent CC clusters.

transformation is given by

$$\Delta Q_{\rm ICM} = \frac{kT_{\rm obs}}{(\gamma-1)}\frac{\Delta K}{K_{\rm g,obs}} \quad \text{(isochoric)}$$
$$= \frac{kT_{\rm obs}}{(1-\frac{1}{\gamma})}\frac{\beta^{2/3}(\beta-1)}{(\beta^{5/3}-1)}\frac{\Delta K}{K_{\rm g,obs}} \quad \text{(isobaric)}, \qquad (7)$$

where $\beta = T_{\rm obs}/T_{\rm th}$. For a value of $\beta = 2$, the ratio between $\Delta Q_{\rm ICM}$ in two cases is 1.14. This implies that if the observed temperature $T_{\rm obs}(m_{\rm g})$ deviates from the theoretically calculated value $T_{\rm th}(m_{\rm g})$ by a factor $\leq$2, then the two above-mentioned estimates of energy input per unit mass differ by only a factor of 1.2. Fig. 2 shows the ratio $\beta = T_{\rm obs}/T_{\rm th}$ for all the clusters and is mostly in the range $0.5 < \beta < 1.2$. We choose the expression for the isobaric process in our estimates. Moreover, we find using isochoric expression instead does not make any notable difference. The total excess energy per particle in ICM can be found by including the change in potential energy term in last equation

$$\Delta E_{\rm ICM} = \Delta Q_{\rm ICM} + G\mu m_{\rm p}\left(\frac{M_{\rm tot}(r_{\rm th})}{r_{\rm th}} - \frac{M_{\rm tot}(r_{\rm obs})}{r_{\rm obs}}\right), \qquad (8)$$

where $r_{\rm th}$ and $r_{\rm obs}$ are theoretical and observed radii respectively enclosing the same gas mass.

The total feedback energy per particle in ICM can be found after adding the energy lost due to cooling i.e.

$$\Delta E_{\rm feedback} = \Delta E_{\rm ICM} + \Delta E_{\rm cool}. \qquad (9)$$

We approximate the energy lost in ICM in a given mass shell as

$$\Delta E_{\rm cool} = \Delta L_{\rm bol}\, t_{\rm age}, \qquad (10)$$

where $\Delta L_{\rm bol}$ is the bolometric luminosity emitted by the ICM in a given shell that is obtained by considering cooling function $\Lambda_{\rm N}$ given in Tozzi & Norman (2001) and $t_{\rm age}$ is the age of the cluster that we have fixed at 5 Gyr (Chaudhuri et al. 2013). $\Lambda_{\rm N}$ is calculated using theoretical (initial) temperature and density profiles. We found using observed profiles instead of theoretical profiles does not make any notable difference in our estimates.

The total amount of energy deposited, for the whole cluster is

$$E_{\rm feedback} = \int \Delta E_{\rm feedback}\frac{1}{\mu_{\rm g} m_{\rm p}}\,{\rm d}m_{\rm g}, \qquad (11)$$

where $\mu_{\rm g} = 0.6$ is the mean molecular weight of gas and $m_{\rm p}$ is mass of proton. Dividing the total energy in the ICM by the total number of particles in the ICM, we estimate the average energy per particle ($\epsilon_{\rm feedback}$).

4 RESULTS AND DISCUSSION

In this section, we study the entropy and energy deposition profiles (in terms of ΔK and $\Delta E_{\rm feedback}$ profiles) in the galaxy clusters up to r_{200} ($m_{\rm g}/m_{\rm g,\,500} = 1.6$) using the methodology discussed in the previous section. We also investigate the impact of the non-thermal pressure, gas clumping and baryonic fraction on our estimates. All the figures that follow assume AMR entropy profiles and *Planck* estimates of the universal baryonic fraction $f_{\rm b} = 0.156$ unless stated otherwise. We shall refer to the case where we assume $f_{\rm b} = 0.156$ and consider both non-thermal pressure and clumping as a fiducial case. The results obtained using SPH baseline entropy profiles are shown in Appendix A.

4.1 ΔK and ΔE profiles

In Fig. 3, we show ΔK profiles of all the individual clusters as a function of $m_{\rm g}/m_{\rm g,\,500}$ and Fig. 4 shows the corresponding $\Delta E_{\rm feedback}$ profiles. The weighted average profiles are shown in the Figs 5 and 6.

In general, we find that for both ΔK and $\Delta E_{\rm feedback}$,

(i) The average profile for full sample is positive in the inner regions, but it becomes negative in the outer regions.

(ii) The inclusion of clumping factor increases overall profiles, due to the increase of observed entropy profiles.

(iii) The inclusion of non-thermal pressure decreases overall profiles up to r_{500} and in the outer radii the profiles actually unexpectedly increase.

(iv) The average profiles of CC and NCC clusters differ significantly. CC clusters have much higher values compared to the average.

Given the negative values of ΔK at the outer radii, the corresponding profiles of ΔE per particle would also be negative. On the face of it, the result would be physically meaningless. However, one should note that ICM gas loses energy due to radiation and the amount of energy lost due to radiation can be added to offset the negative values. Solid red line and dashed red line in Fig. 5 show the average profiles with and without taking into account energy lost due to cooling, respectively. The difference in these two curves is small beyond r_{500} because of the fact that gas density is small in those regions and therefore radiative cooling cannot explain the profiles going below zero in the outer region.

Tables 2 and 3 give the estimates of average feedback energy per particle $\epsilon_{\rm feedback}$ in the ranges $0.2r_{500}$–r_{500}, $0.2r_{500}$–r_{200} and r_{500}–r_{200} using *Planck* and *WMAP* estimates of the baryonic fraction. It can be seen that the inclusion of non-thermal pressure affects the estimates of $\epsilon_{\rm feedback}$ both in the inner and outer regions of the cluster and that clumping has a substantial effect only in the cluster outer regions. In the next two subsections, we show as to how the proper incorporation of both clumping and non-thermal pressure can lead to meaningful estimates of the feedback profiles.

4.2 Importance of gas clumping

In the outer regions, the level of clumping in gas profile can be significant which can also lead to biased estimates of density and hence in entropy measurements. Fig. 6 shows the comparison of

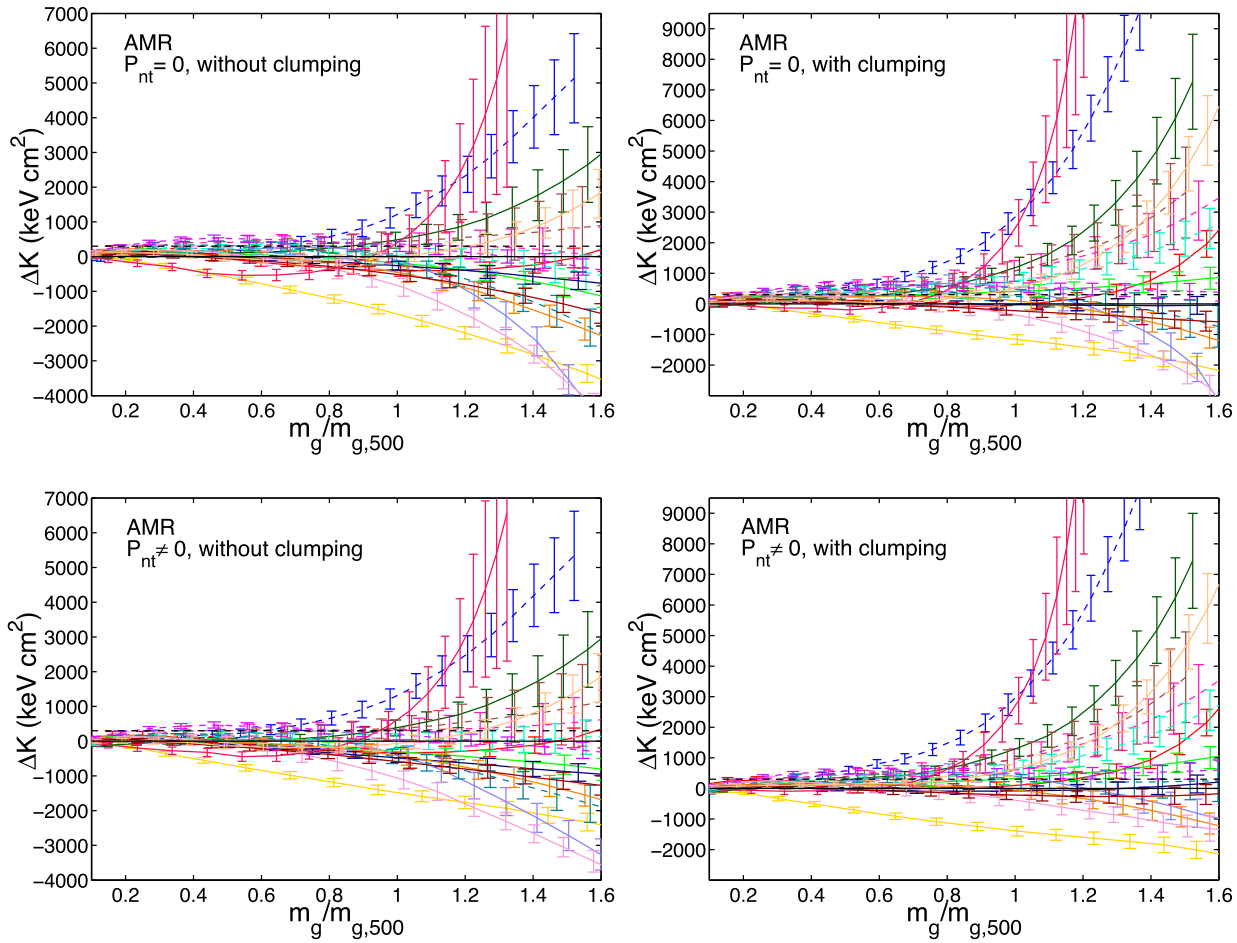

Figure 3. Excess entropy ΔK as a function $m_g/m_{g,500}$ using benchmark AMR entropy profile. Left-hand panel: without clumping, right-hand panel: with clumping. Upper panel: $P_{nt} = 0$, lower panel: $P_{nt} \neq 0$. Thin dashed lines represent NCC clusters and dashed red lines represent CC clusters. The error bars are given at 1σ level. Note that for meaningful comparison, we have scaled x-axis of all cases with same $m_{g,500}$ as that of fiducial case (i.e. with clumping and $P_{nt} \neq 0$).

average ΔK and $\Delta E_{feedback}$ profiles for various cases. One can clearly see the implications of correcting the entropy by using the clumping profile from Eckert et al. (2015) on our estimates. The addition of clumping factor raises ΔK and hence $\Delta E_{feedback}$ profiles as expected. Here, the increase is not negligible and makes the average profile become more or less consistent with zero in the outer regions for $P_{nt} \neq 0$ case. However, for the pure thermal case, the profiles are still negative in the outer regions to a significant level which we ascribe to the neglect of non-thermal pressure in the next subsection.

Comparing the average ΔK feedback profiles with and without clumping, one can see that ignoring the clumping correction leads to a decrease of $\Delta K \approx 300$ keV cm^2 at r_{500} and $\Delta K \approx 1100$ keV cm^2 at r_{200}. The energy feedback profiles on the other hand are underestimated by $\Delta E_{feedback} \approx 1$ keV at r_{500} and $\Delta E_{feedback} \approx 1.5$ keV at r_{200}. Similarly, from Tables 2 and 3, it is also evident that the average feedback energy per particle, $\epsilon_{feedback}$, is underestimated by 0.5 keV in the region $0.2r_{500}$–r_{500} and 1.2 keV in the region r_{500}–r_{200} if clumping correction is neglected.

4.3 Importance of non-thermal pressure

Although, the inclusion of the non-thermal pressure decreases the feedback profiles up to r_{500} due to the overall increase in the normalization (K_{200}) in the benchmark entropy profiles; however, as seen from Fig. 6, it unexpectedly increases beyond that. The cross-over occurs around (1.1–1.2)r_{500}. This can be understood as follows: Due to the neglect of the non-pressure, the M_{tot} profile is underestimated which in turn results in the underestimation of theoretical gas mass as $f_{g,th} = 0.9 f_b$ is fixed at the virial radius. This implies for the given observed gas mass shell the corresponding theoretical gas mass for $P_{nt} = 0$ case will occur at larger radius as compared to $P_{nt} \neq 0$ case and will, therefore, have higher theoretical entropy leading to decrease in feedback profiles. Below r_{500}, the increase in K_{200} term dominates (since non-thermal pressure is small) and therefore, there is an overall decrease in the feedback profiles for $P_{nt} \neq 0$ case.

From Fig. 6, it is evident that ignoring the non-thermal pressure leads to an overestimation of $\Delta K \approx 100$ keV cm^2 at r_{500} and underestimation of $\Delta K \approx 450$ keV cm^2 at r_{200}. This in turn leads to an overestimation of $\Delta E \approx 0.5$ keV at r_{500} and underestimation of $\Delta E \approx 0.25$ keV at r_{200}. Similarly, one can see from Tables 2 and 3, if non-thermal pressure is ignored then the $\epsilon_{feedback}$ is overestimated by 0.6 keV in the region $0.2r_{500}$–r_{500} while it has a negligible effect in the region r_{500}–r_{200}.

In Fig. 7, we show the effect on the feedback profile by changing the normalization a_0 and slope n_{nt} in the non-thermal pressure. We find that changing the normalization from 0.18 to (0.10, 0.26) gives around (10 per cent, 30 per cent) mass difference at r_{500}. The

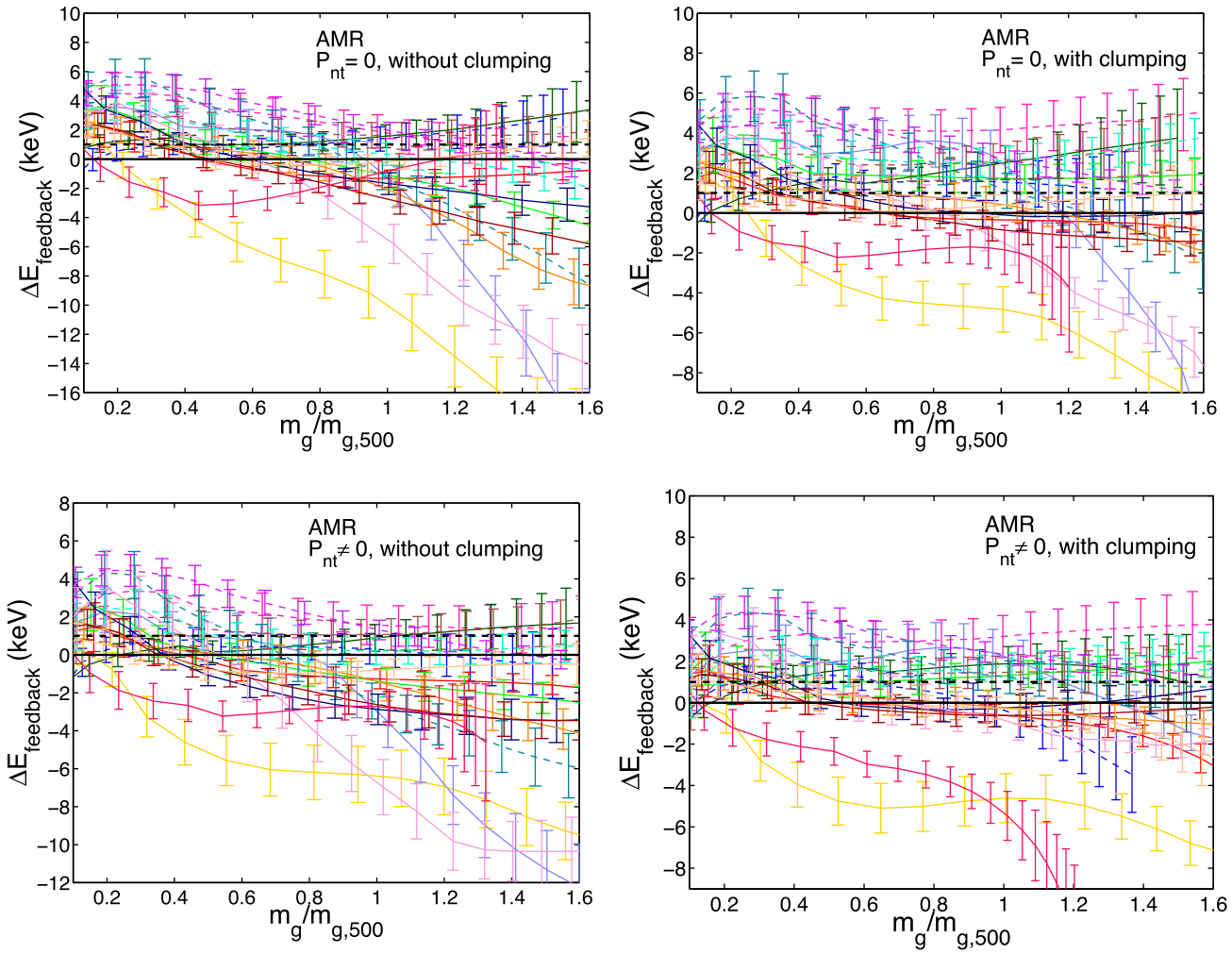

Figure 4. Excess energy per particle ΔE as a function $m_{\rm g}/m_{\rm g,\,500}$ using benchmark AMR entropy profile. Left-hand panel: without clumping, right-hand panel: with clumping. Upper panel: $P_{\rm nt} = 0$, lower panel: $P_{\rm nt} \neq 0$. Thin solid lines represent NCC clusters and dashed lines represent CC clusters. The error bars are given at 1σ level. Note that for meaningful comparison, we have scaled x-axis of all cases with same $m_{\rm g,\,500}$ as that of fiducial case (i.e. with clumping and $P_{\rm nt} \neq 0$).

change in normalization and slope has a small effect on the profiles and our results are still consistent with zero line given the error bars. We also observe that other parametrization of non-thermal pressure such as that of Shi et al. (2015) and Rasia et al. (2004) lies within the normalization 0.10–0.26 band of our non-thermal pressure model. Therefore, our results are independent of the non-thermal parametrization.

5 ROBUSTNESS OF RESULTS

5.1 CC and NCC clusters

Fig. 8 shows the ΔK and $\Delta E_{\rm feedback}$ profiles for CC and NCC populations with and without taking into account $P_{\rm nt}$+clumping. The higher value of ΔK and $\Delta E_{\rm feedback}$ profiles for CC clusters can be interpreted in terms of the gas mass fraction. Eckert et al. (2013b) found that the observed gas mass fraction profile in the CC clusters was systematically lower than NCC clusters. Since, the theoretical value $f_{\rm g,th}$ is fixed at $0.9f_{\rm b}$ at virial radius and the observed value of $f_{\rm g,obs}$ for CC clusters is relatively smaller than NCC clusters, this means that for a given observed gas mass $m_{\rm g,obs}$, the corresponding theoretical gas $m_{\rm g,th}$ for CC clusters will also occur at a relatively smaller radius with a smaller value of theoretical entropy. This will thus result in a relatively higher degree of feedback and up to a much larger radii in CC clusters compared to NCC clusters.

Higher estimates of the feedback profiles in the CC clusters can be due to larger rate of gas removal as a result cooling and simultaneous inflow of high entropy gas to the cluster cores (a sort of 'cooling flow'). Moreover, removal of gas due to cooling that corresponds to stellar formation also changes the mapping of the observed gas mass enclosed with radius to the mass shell in the theoretical prediction. This could again contribute to the apparent entropy excess in CC clusters relative to NCC clusters especially in the cluster cores. However, the replacement of cool gas with gas at high entropy occurs mostly in the inner region (few hundred kpc) which we have not considered in our analysis, and is unlikely to cause much difference.

Another potential origin of the apparent entropy excess in CC clusters could be due to the differences in the shape of the non-thermal pressure profile. Since cool-core clusters tend to have more relaxed centres than NCC clusters, steeper gradient would lead to an overestimation of total mass and hence a smaller value of observed gas fraction. However, this should compensate with the higher gas density of CC clusters in the inner regions. Moreover, as can be seen

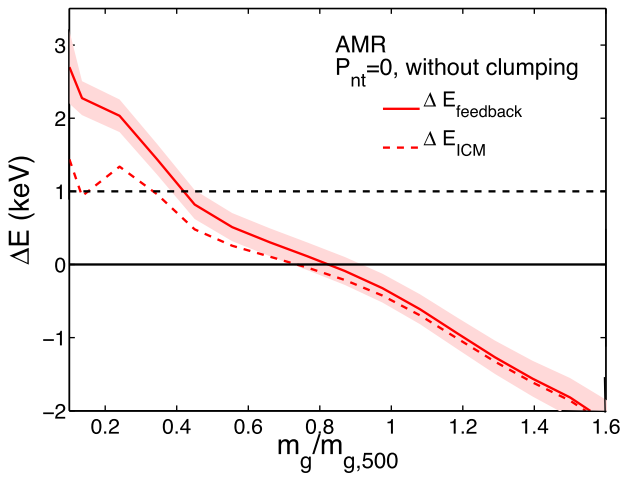

Figure 5. The average ΔE profile for the entire sample with and without adding energy lost due to cooling.

from Fig. 7 the change in normalization and slope of the non-thermal pressure has a small effect in the feedback profiles suggesting this is not the case.

5.2 Full sample and sub-sample

There are four clusters (i.e clusters 1, 6, 16 and 17) that have relatively large value of the ΔK profile in the outer regions (particularly for the clumping case) that correspondingly give a large thermal energy profile $\Delta Q_{\rm ICM}$. However, we see that after taking into account a potential energy term the $\Delta E_{\rm feedback}$ profiles for such clusters become close to zero (or even negative). In order to see the effect of such clusters, we have plotted in Fig. 9 average ΔK and $\Delta E_{\rm feedback}$ profiles for the full sample along with the sub-sample which do not include these clusters. We find that the average feedback entropy become consistent with $\Delta K \approx 0$ line at 1σ beyond r_{500} for the sub-sample. Moreover, average ΔK and $\Delta E_{\rm feedback}$ profiles for the sub-sample and full sample are always consistent with one another.

5.3 Choice of boundary condition

In Fig. 10, we show the comparison of the entropy feedback profiles for two different boundary conditions, i.e. universal baryonic fraction $f_{\rm b}$ at virial radius to be 0.156 (from *Planck*) and 0.167 (from *WMAP*). The larger value of the $f_{\rm b}$ from *WMAP* would result in an overall increase of feedback profiles. This is because higher value of $f_{\rm b}$ at the virial radius will increase the total theoretical gas mass profile (as total mass remains constant). Therefore, a given theoretical gas mass shell would occur at a smaller radius having a lower value of entropy leading to an increase in feedback profiles. It is clear from Fig. 10 that the entropy feedback profiles for the *WMAP* boundary conditions is significantly higher at the outer regions ($\Delta K \approx 300\,{\rm keV\,cm^2}$).

5.4 Choice of observed X-ray profiles – parametric versus deprojected

Eckert et al. (2013a) found that the parametric and deprojected density profiles are similar and the difference is less than 10 per cent. We show the ΔK profiles for all the clusters using deprojected data in Fig. 11. We find parametric and deprojected profiles have similar values of entropy difference from the base theoretical entropy profiles except at the cluster outskirts.

6 AMR VERSUS SPH BENCHMARK THEORETICAL PROFILE

Given the current status, it is difficult to judge whether SPH or AMR is more accurate since both these methods are known to have some demerits. For example SPH suffers from a relatively poor shock resolution and noise on the scale of the smoothing kernel. AMR simulations may suffer from overmixing due to advection

Table 2. Average feedback energy per particle $\epsilon_{\rm feedback}$ for AMR case with *Planck* $f_{\rm b} = 0.156$.

		Energy per particle (keV)					
		Without cooling energy			With cooling energy		
C	P_{nt}	0.2–1r_{500}	0.2–1r_{200}	r_{500}–r_{200}	0.2–1r_{500}	0.2–1r_{200}	r_{500}–r_{200}
				Full sample			
0	0	0.39 ± 0.20	−0.29 ± 0.21	−1.33 ± 0.23	0.80 ± 0.20	−0.02 ± 0.21	−1.27 ± 0.23
0	Nonzero	−0.31 ± 0.19	−0.73 ± 0.20	−1.35 ± 0.21	0.09 ± 0.19	−0.46 ± 0.20	−1.29 ± 0.21
Nonzero	0	0.91 ± 0.18	0.60 ± 0.19	0.06 ± 0.20	1.29 ± 0.18	0.85 ± 0.19	0.11 ± 0.20
Nonzero	Nonzero	0.35 ± 0.17	0.23 ± 0.17	0.03 ± 0.18	0.72 ± 0.17	0.46 ± 0.17	0.05 ± 0.18
				NCC clusters			
0	0	−0.25 ± 0.24	−1.08 ± 0.26	−2.35 ± 0.30	0.16 ± 0.24	−0.80 ± 0.26	−2.28 ± 0.30
0	Nonzero	−0.97 ± 0.23	−1.51 ± 0.25	−2.35 ± 0.27	−0.56 ± 0.23	−1.24 ± 0.25	−2.28 ± 0.27
Nonzero	0	0.27 ± 0.24	−0.15 ± 0.27	−0.88 ± 0.30	0.65 ± 0.24	0.09 ± 0.27	−0.82 ± 0.30
Nonzero	Nonzero	−0.21 ± 0.23	−0.42 ± 0.25	−0.76 ± 0.27	0.15 ± 0.23	−0.17 ± 0.25	−0.71 ± 0.27
				CC clusters			
0	0	1.73 ± 0.38	1.06 ± 0.38	0.11 ± 0.36	2.14 ± 0.38	1.32 ± 0.38	0.16 ± 0.36
0	Nonzero	1.03 ± 0.36	0.63 ± 0.35	0.12 ± 0.33	1.44 ± 0.36	0.89 ± 0.35	0.17 ± 0.33
Nonzero	0	2.52 ± 0.39	2.36 ± 0.41	2.02 ± 0.44	2.88 ± 0.39	2.60 ± 0.41	2.06 ± 0.44
Nonzero	Nonzero	2.20 ± 0.41	1.97 ± 0.41	1.68 ± 0.34	2.60 ± 0.41	2.23 ± 0.41	1.73 ± 0.41

Columns (3)–(5): $\epsilon_{\rm feedback}$ in the ranges (0.2–1)r_{500}, (0.2–1)r_{200} and r_{500}–r_{200} respectively without taking into account energy lost due to cooling. Columns (6)–(8): $\epsilon_{\rm feedback}$ in the ranges (0.2–1)r_{500}, (0.2–1)r_{200} and r_{500}–r_{200} respectively after taking into account energy lost due to cooling. The errors are given at 1σ level. For meaningful comparison, $\epsilon_{\rm feedback}$ for $P_{\rm nt} = 0$ case are also calculated up to same radii as that of non-thermal case (i.e.r_{500} and r_{200} of $P_{\rm nt} \neq 0$).

Table 3. Average feedback energy per particle $\epsilon_{\rm feedback}$ for AMR case with *WMAP* $f_{\rm b} = 0.167$.

		Energy per particle (keV)					
		Without cooling energy			With cooling energy		
C	$P_{\rm nt}$	$0.2–1r_{500}$	$0.2–1r_{200}$	$r_{500}–r_{200}$	$0.2–1r_{500}$	$0.2–1r_{200}$	$r_{500}–r_{200}$
				Full sample			
0	0	0.89 ± 0.20	0.22 ± 0.21	−0.79 ± 0.21	1.30 ± 0.20	0.49 ± 0.21	−0.72 ± 0.21
0	Nonzero	0.17 ± 0.19	−0.22 ± 0.19	−0.83 ± 0.20	0.58 ± 0.19	0.04 ± 0.19	−0.77 ± 0.20
Nonzero	0	1.35 ± 0.19	1.11 ± 0.19	0.71 ± 0.19	1.73 ± 0.19	1.37 ± 0.19	0.76 ± 0.19
Nonzero	Nonzero	0.72 ± 0.18	0.66 ± 0.17	0.56 ± 0.17	1.10 ± 0.18	0.89 ± 0.17	0.59 ± 0.17
				NCC clusters			
0	0	0.26 ± 0.24	−0.56 ± 0.26	−1.83 ± 0.26	0.68 ± 0.26	−0.28 ± 0.26	−1.70 ± 0.29
0	Nonzero	−0.45 ± 0.23	−0.99 ± 0.24	−1.83 ± 0.25	−0.04 ± 0.23	−0.72 ± 0.24	−1.76 ± 0.25
Nonzero	0	0.73 ± 0.25	0.41 ± 0.26	−0.12 ± 0.29	1.11 ± 0.25	0.67 ± 0.26	−0.07 ± 0.29
Nonzero	Nonzero	0.16 ± 0.24	0.05 ± 0.25	−0.11 ± 0.26	0.54 ± 0.24	0.30 ± 0.25	−0.06 ± 0.26
				CC clusters			
0	0	2.28 ± 0.38	1.69 ± 0.38	0.88 ± 0.36	2.69 ± 0.38	1.94 ± 0.38	0.93 ± 0.36
0	Nonzero	1.55 ± 0.36	1.22 ± 0.35	0.77 ± 0.32	1.96 ± 0.36	1.48 ± 0.35	0.82 ± 0.32
Nonzero	0	2.98 ± 0.40	2.88 ± 0.42	2.68 ± 0.45	3.34 ± 0.40	3.12 ± 0.42	2.72 ± 0.45
Nonzero	Nonzero	2.70 ± 0.41	2.53 ± 0.42	2.33 ± 0.42	3.10 ± 0.41	2.80 ± 0.42	2.38 ± 0.42

Columns (3)–(5): $\epsilon_{\rm feedback}$ in the ranges $(0.2–1)r_{500}$, $(0.2–1)r_{200}$ and $r_{500}–r_{200}$ respectively without taking into account energy lost due to cooling. Columns (6)–(8): $\epsilon_{\rm feedback}$ in the ranges $(0.2–1)r_{500}$, $(0.2–1)r_{200}$ and $r_{500}–r_{200}$ respectively after taking into account energy lost due to cooling. The errors are given at 1σ level. For meaningful comparison, $\epsilon_{\rm feedback}$ for $P_{\rm nt} = 0$ case are also calculated up to same radii as that of non-thermal case (i.e. r_{500} and r_{200} of $P_{\rm nt} \neq 0$).

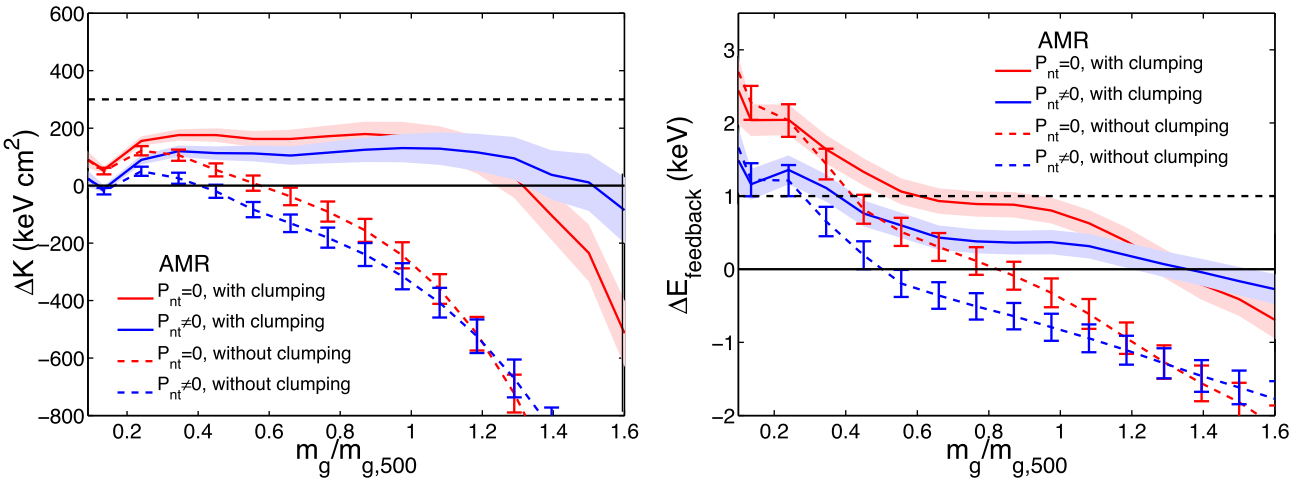

Figure 6. Comparison of average ΔK and ΔE profiles for different cases considered in this work. The error bars are given at 1σ level.

errors in the presence of bulk flows. Apart from the slightly smaller normalization of the entropy profile a_0, the AMR simulations predict a much higher flatter entropy core than the corresponding SPH simulations (Voit et al. 2005). However, it has been recently pointed out by many authors that, after resolving certain hydrodynamic processes, the results of SPH simulations exactly match with AMR simulations (Mitchell et al. 2009; Vazza et al. 2011; Valdarnini 2012; Power et al. 2014; Biffi & Valdarnini 2015). We nevertheless use SPH-simulated entropy in our estimates to compare it with that of AMR case. The feedback profiles and feedback energy per particle for SPH case are shown in the Figs A1 and A2 and Tables A1 and A2 respectively in Appendix A. In Fig. 12, we compare the average excess entropy and energy profiles for both AMR and SPH cases. As can be seen, SPH case predicts much higher values of ΔE in the inner regions of the cluster because of the absence of flatter entropy profile as is present in AMR case.

The ΔK and $\Delta E_{\rm feedback}$ feedback profiles at the outer radii contain information of past events in the cluster and hence are ideal to probe for any signature of pre-heating that may have taken place at high redshifts much before the cluster formation. This is because of the fact that feedback processes from AGNs or supernovae are unlikely to affect the gas properties there. However, we should also point that our estimated $\Delta E_{\rm feedback}$ profiles correspond to the change from the initial theoretical model to the observed configuration in the collapsed systems. Pre-heating (if any) at high redshift when the density of gas was small would actually require much smaller energy input to bring it to final observed state (McCarthy et al. 2008). Therefore, $\Delta E_{\rm feedback}$ would represent an upper limit on pre-heating energy.

It has been found that pre-heating scenarios (at $z \approx 4–6$) typically require feedback energy of $\sim$1 keV per particle or an entropy floor of $>$300 keV cm^2 to explain break in the self-similarity scaling relations (Borgani et al. 2001; Tozzi & Norman 2001; Pipino et al. 2002;

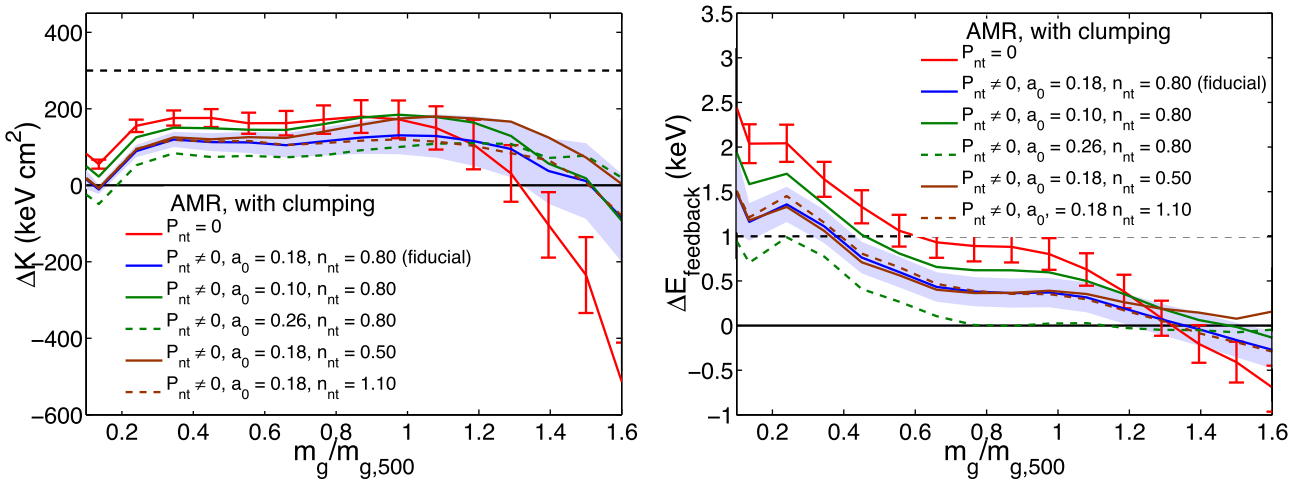

Figure 7. Comparison of feedback profiles for different parametrizations of $P_{\rm nt}$. The error bars are given at 1σ level.

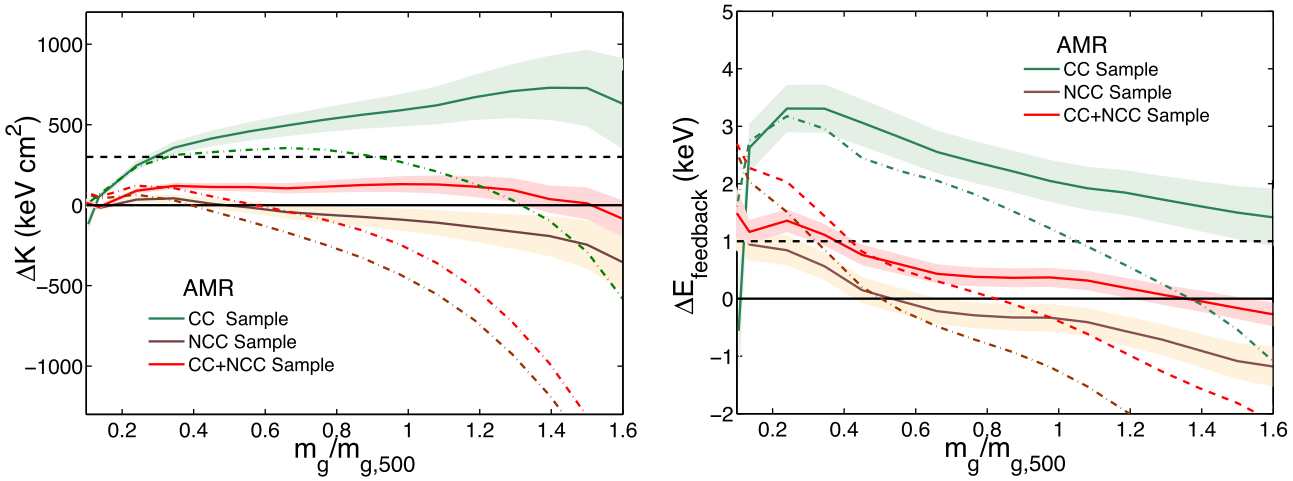

Figure 8. Comparison between CC clusters and NCC clusters. The solid lines with error bars represent feedback profiles with $P_{\rm nt}$ and clumping included and dashed dotted lines (without error bars) represent a case where we do not take $P_{\rm nt}$ and clumping into account. The error bars are given at 1σ level.

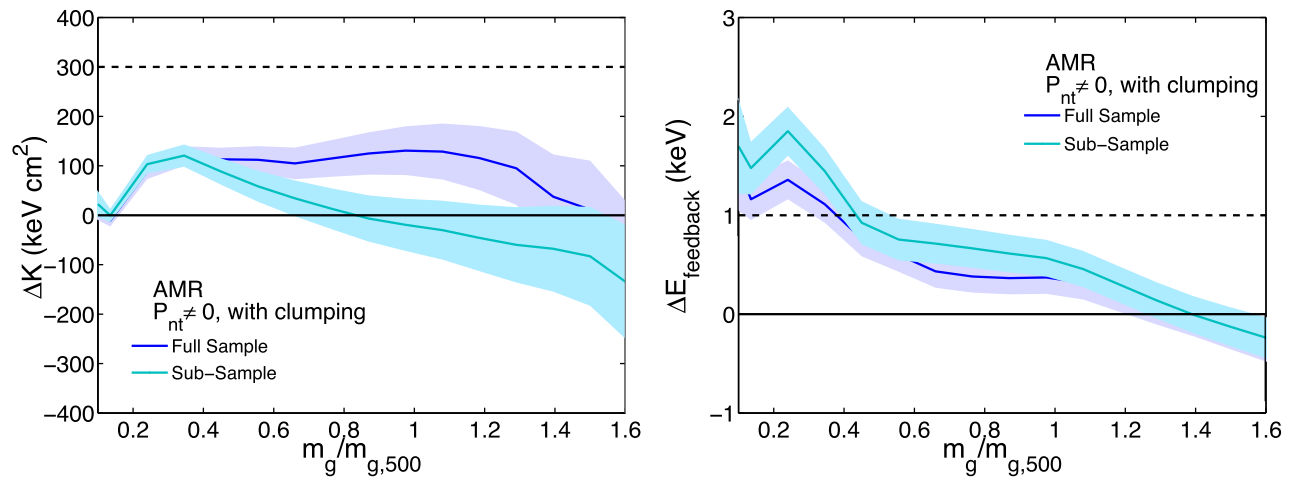

Figure 9. Comparison of feedback profiles for sub-sample and full sample. The error bars are given at 1σ level.

Finoguenov et al. 2003). Our results show that given the uncertainties, the values of ΔE at the outer radii are comparable to zero for both AMR and SPH cases (see Fig. 12). For our fiducial case, we see that in the range r_{500}–r_{200}, the average energy per particle $\epsilon_{\rm feedback} = 0.05 \pm 0.18$ for the AMR case and $\epsilon_{\rm feedback} = 0.62 \pm 0.18$ for SPH case. This implies that pre-heating scenarios that predict 1 keV energy per particle are ruled out with more than 3σ for AMR case and at around 2σ for SPH case. Considering ΔK profiles, we

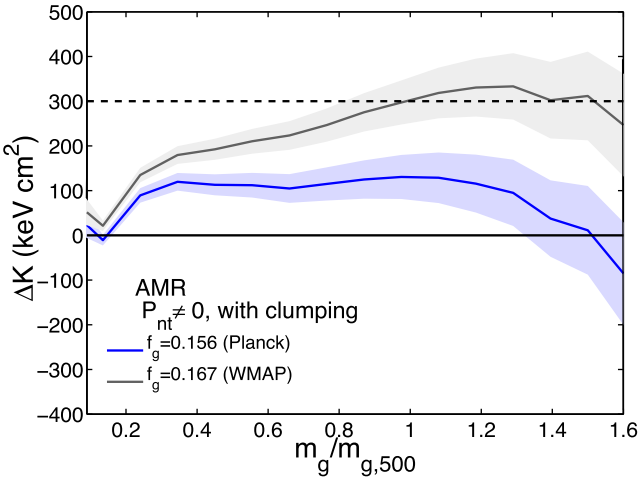

Figure 10. The average ΔK feedback profiles as a function of $m_{\rm g}/m_{\rm g,\,500}$ for two boundary conditions of gas fraction at virial radius (i.e. $f_{\rm b} = 0.156$ from *Planck* and $f_{\rm b} = 0.167$ from *WMAP*).

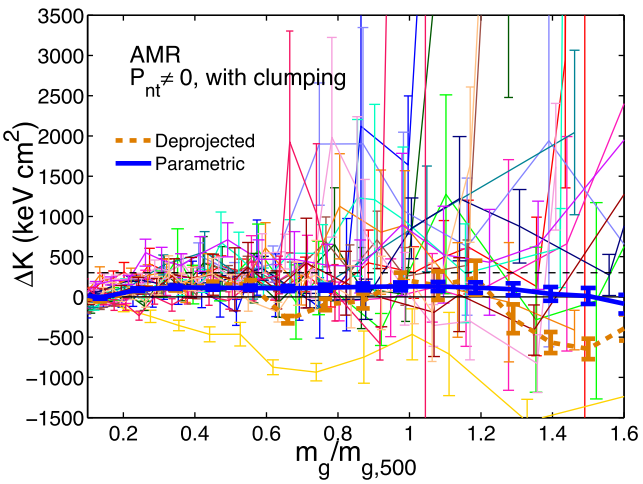

Figure 11. The average ΔK feedback profiles as a function of $m_{\rm g}/m_{\rm g,\,500}$ for all the clusters considering the deprojected case.

find for most of the cluster region an entropy floor >300 keV cm^2 is ruled out at $\approx 3\sigma$ for the AMR case. However, no such strong constrains are possible for the SPH case and that $\Delta K \approx 300$ keV cm^2 is consistent with 1σ as seen in the left-hand side of Fig. 12.

7 COMPARISON WITH PREVIOUS RESULTS

It is important to distinguish between the profiles of K with respect to shells at fixed position (Pratt et al. 2010; Ettori 2013), and with respect to shells with a given gas mass interior to it (Nath & Majumdar 2011; Chaudhuri et al. 2012, 2013). This aspect is demonstrated in Fig. 13. The right-hand panel shows the entropy profiles with respect to fixed radii, and the left-hand panel shows the entropy with respect to shells with a given gas mass interior to it. The differences between the profiles (w.r.t. r/r_{500} and $m_{\rm g}/m_{\rm g,\,500}$) are striking and noteworthy. The observed entropy profiles (solid brown line) show an enhancement of entropy in the inner region, but drop below the theoretical profile in the outer region. In this case, the inclusion of non-thermal pressure would seem to exacerbate the situation and the deviation of observed profile becomes acute. However, one see that after accounting for the clumping correction, the recovered entropy profiles (solid black line) show an excess compared to theoretical entropy profile with respect to gas mass for most of the cluster region. Comparing entropy profiles at the same radii, we find the deviations between theoretical and clumping corrected entropy profiles become negligible beyond $0.5r_{500}$. It is also worth mentioning here that for theoretical entropy profiles the cross-over between $P_{\rm nt} = 0$ and $P_{\rm nt} \neq 0$ cases is around $(1.1\text{–}1.2)r_{500}$ as also seen in average ΔK and ΔE profiles (see Fig. 6).

Earlier, Chaudhuri et al. (2013) determined the feedback profile up to r_{500}. They found total feedback energy $E_{\rm feedback}$ scales with the mean spectroscopic temperature as $E_{\rm feedback} \propto T^{2.52\,\pm\,0.08}$ and $E_{\rm feedback} \propto T^{2.17\,\pm\,0.11}$ for the SPH and AMR baseline profiles, respectively. They showed that $E_{\rm feedback}$ correlates strongly with the radio luminosity $L_{\rm R}$ of the central radio sources and estimated energy per particle to be 2.8 ± 0.8 keV for the SPH simulations and 1.7 ± 0.9 keV for the AMR simulations which is much greater than our estimate. Notice that they did not consider non-thermal pressure and clumping and their calculations included cluster cores which results in the higher estimates of energy per particle.

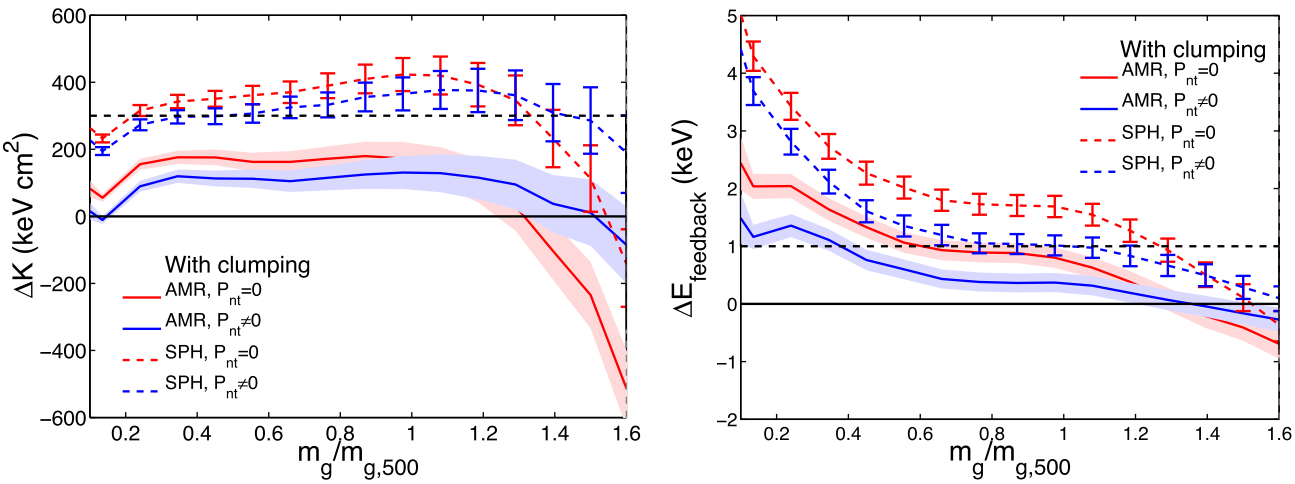

Figure 12. Comparison of feedback profiles for AMR and SPH cases. For meaningful comparison, we have scaled x-axis of all with same $m_{\rm g,\,500}$ as that of fiducial case (i.e. with clumping and $P_{\rm nt} \neq 0$).

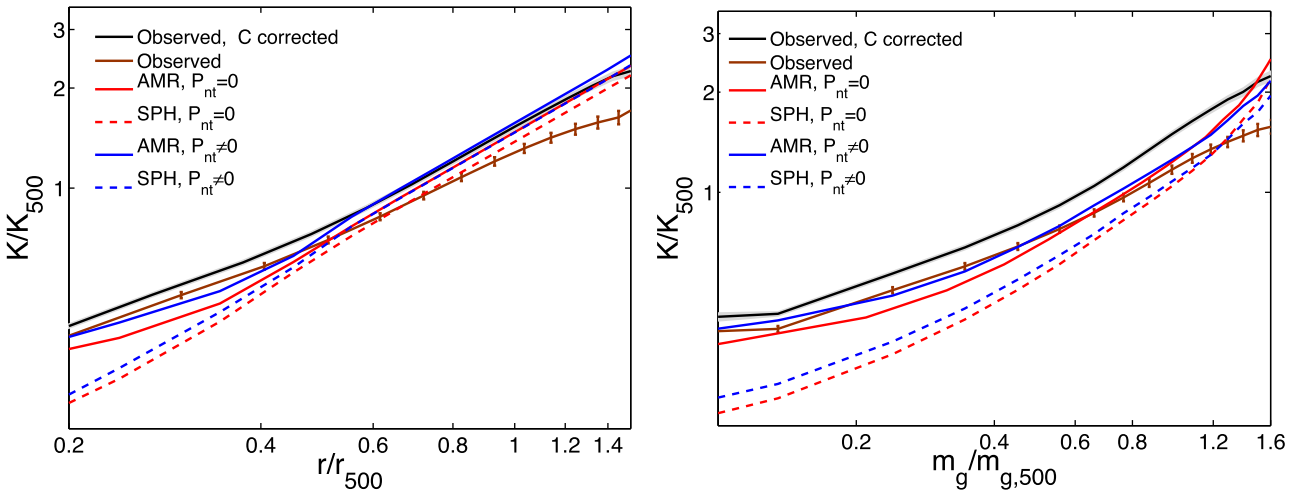

Figure 13. Comparison between entropy profiles with respect to fixed radii (left-hand panel) and with respect to shells with a given gas (right-hand panel). The observed average entropy profiles with and without clumping correction are shown in black and brown lines, whereas theoretical profiles with and without non-thermal pressure are shown in blue and red lines, respectively. Note that for meaningful comparison, we have scaled K, $m_{\rm g}$ and r with same K_{500}, $m_{\rm g,\,500}$ and r_{500} as that of fiducial case (i.e. with clumping and $P_{\rm nt} \neq 0$).

8 CONCLUSIONS

Recent studies have revealed that non-gravitational processes play an important role in modifying the thermodynamic properties of the ICM. It has also been observed that there is an entropy enhancement in galaxy clusters which is believed to be a result of the non-gravitational feedback from active galactic nuclei, radiative cooling, supernovae, etc. We have studied the fractional entropy enhancement and the corresponding feedback energy in the ICM for a sample of 17 galaxy clusters by comparing the observed entropy profiles with that of AMR and SPH non-radiative simulations. Unlike, previous work by Chaudhuri et al. (2013) where they estimated the feedback energetics up to radius $\lesssim r_{500}$, our study goes up to r_{200}. Since around 30 per cent of the total cluster mass (and almost 80 per cent of the cluster volume) is outside of r_{500}, this study has important implication on the ICM thermodynamics and feedback processes. The cluster outskirts have many features that are not significant into cluster cores. These include deviation from the hydrostatic equilibrium and gas clumping. Therefore, our analysis takes both non-thermal pressure and clumping into account which are important to study the energetics of ICM in the outer regions.

We show that neglect of clumping and non-thermal pressure can lead to an underestimation of r_{500} and r_{200} by 1–20 per cent. Similarly, we find an under/overestimation of feedback profiles. We find that the effect of clumping is much more pronounced than the non-thermal pressure and neglecting it always leads to an underestimation of feedback profiles. The neglect of clumping leads to an underestimation of entropy $\Delta K \approx 1100\,{\rm keV\,cm^2}$ and feedback energy per particle $\Delta E_{\rm feedback} \approx 1\,{\rm keV}$ at r_{200}. The neglect of non-thermal pressure on the other hand leads to an overestimation in the inner regions and underestimation in the outer regions. The omission of the non-thermal pressure results in an underestimation of entropy $\Delta K \approx 450\,{\rm keV\,cm^2}$ and feedback energy per particle $\Delta E_{\rm feedback} \approx 0.25\,{\rm keV}$ at r_{200}. Further, we find that the feedback energy profiles are centrally peaked which can be related with AGN feedback models and more or less flatten out in the outer regions becoming consistent with zero.

Finally, to check the robustness of our results, we compared the feedback profiles for different cases: CC and NCC clusters, the full sample and a sub-sample, parametric and deprojected cases. We find the much higher value of feedback profiles for the CC clusters compared to NCC clusters. However, since CC clusters comprise a much smaller sample one, therefore, needs to improve/verify the estimates by considering a larger sample. We also find that the choice of the universal baryonic fraction from *WMAP* and *Planck* can have implications on the estimates of the feedback profiles.

In order to obtain any robust estimates of cosmological parameters from large SZ surveys and SZ power spectrum, one needs to properly incorporate the non-gravitational feedback. Therefore, it is utmost important to understand the nature and extent of the non-gravitational feedback in galaxy clusters, out to the virial radius, so as to properly calibrate the scaling relations and theoretical cluster models. In principle, one can consider different parametrizations of excess entropy and feedback energy to see the effects of the non-gravitational feedback on ICM thermodynamics.

ACKNOWLEDGEMENTS

This work was supported by SERB (DST) Project Grant No. SR/S2/HEP-29/2012. AI would like to thank Tata Institute of Fundamental Research (TIFR), Mumbai and Raman Research Institute (RRI), Bangalore for hospitality.

REFERENCES

Arnaud M., Pratt G. W., Piffaretti R., Böhringer H., Croston J. H., Pointecouteau E., 2010, A&A, 517, 20
Battaglia N., Bond J. R., Pfrommer C., Sievers J. L., 2012, ApJ, 758, 74
Battaglia N., Bond J. R., Pfrommer C., Sievers J. L., 2015, ApJ, 806, 43
Biffi V., Valdarnini R., 2015, MNRAS, 446, 2802
Birzan L., Rafferty D. A., Namara B. R., Wise M. W., Nulsen P. E. J., 2004, A&A, 469, 363
Borgani S. et al., 2001, ApJ, 559, 71
Bryan G. L., Norman M. L., 1998, ApJ, 495, 80
Cavagnolo K. W., Donahue M., Voit G. M., Sun M., 2009, ApJS, 182, 12
Cavaliere L., Lapi A., Fusco-Femiano R., 2011, ApJ, 742, 19
Chaudhuri A., Nath B. B., Majumdar S., 2012, ApJ, 759, 5
Chaudhuri A., Majumdar S., Nath B. B., 2013, ApJ, 776, 84
Crain R. A., Eke V. R., Frenk C. S., Jenkins A., McCarthy I. G., Navarro J. F., Pearce F. R., 2007, MNRAS, 377, 41
David L. P., Jones C., Forman W., 1996, ApJ, 473, 692

Eckert D. et al., 2012, A&A, 541, A57
Eckert D., Molendi S., Vazza F., Ettori S., Paltani S., 2013a, A&A, 551, A22
Eckert D., Ettori S., Molendi S., Vazza F., Paltani S., 2013b, A&A, 551, A23
Eckert D., Roncarelli M., Ettori S., Molendi S., Vazza F., Gastaldello F., Rossetti M., 2015, MNRAS, 447, 2198
Edge A. C., Stewart G. C., 1991, MNRAS, 252, 414
Ettori S., 2013, MNRAS, 435, 1265
Ettori S., 2015, MNRAS, 446, 2629
Finoguenov A., Borgani S., Tornatore L., Bohringer H., 2003, A&A, 398, 35
Fujita Y., Ohira Y., Yamazaki R., 2013, ApJ, 767, L4
Fusco-Femiano R., Lapi A., 2013, ApJ, 771, 102
Fusco-Femiano R., Lapi A., 2014, ApJ, 783, 76
Gaspari M., Brighenti F., D'Ercole A., Melioli C., 2011, MNRAS, 415, 1549
Gaspari M., Ruszkowski M., Sharma P., 2012, ApJ, 746, 94
Gaspari M., Brighenti F., Temi P., Ettori S., 2014, ApJ, 783, L10
Gladders M. D., Yee H. K. C., Majumdar S., Barrientos L. F., Hoekstra H., Hall P. B., Infante L., 2007, ApJ, 655, 128
Holder G., Haiman Z., Mohr J. J., 2001, ApJ, 560, L111
Holder G. P., Carlstrom J. E., 2001, ApJ, 558, 515
Hoshino A. et al., 2010, PASJ, 62, 371
Iqbal A., Majumdar S., Nath B. B., Ettori S., Eckert D., Malik M. A., 2017, MNRAS, 465, L99
Kaiser N., 1986, MNRAS, 222, 323
Kriss G. A., Cioffi D. F., Canizares C. R., 1983, ApJ, 272, 439
Lau E. T., Kravtsov A. V., Nagai D., 2009, ApJ, 705, 1129
Li R., Mo H. J., Fan Z., van den Bosch F. C., Yang X., 2011, MNRAS, 413, 3039
Li Y., Bryan G. L., Ruszkowski M., Voit G. M., O'Shea B. W., Donahue M., 2015, 811, 73
Markevitch M., 1998, ApJ, 504, 27
Mathiesen B., Evrard A. E., Mohr J. J., 1999, ApJ, 520, L21
McCarthy I. G., Babul A., Bower R. G., Balogh M. L., 2008, MNRAS, 386, 1309
McCarthy I. G., Le Brun A. M. C., Schaye J., Holder G. P., 2014, 440, 3645
McLaughlin D. E., 1999, AJ, 117, 2398
McNamara B. R., Nulsen P. E. J., 2007, ARA&A, 45, 117
Mitchell N. L., McCarthy I. G., Bower R. G., Theuns T., Crain R. A., 2009, MNRAS, 395, 180
Nagai D., Kravtsov A. V., Vikhlinin A., 2007, ApJ, 668, 1
Nagai D., Lau E. T., 2011, ApJ, 731, L10
Nath B. B., Majumdar S., 2011, MNRAS, 416, 271
Pipino A., Matteucci F., Borgani S., Biviano A., 2002, New Astron., 7, 227
Planck Collaboration XI, 2011, A&A, 536, A11
Planck Collaboration III, 2013a, A&A, 550, A129
Planck Collaboration V, 2013b, A&A, 550, A131
Planck Collaboration XX, 2014, A&A, 571, A20
Planck Collaboration XIII, 2015, A&A, 594, A20
Pointecouteau E., Arnaud M., Pratt G. W., 2005, A&A, 435, 1
Ponman T. J., Cannon D. B., Navarro J. F., 1999, Nature, 6715, 135
Power C., Read J. I., Hobbs A., 2014, MNRAS, 440, 3243
Pratt G. W., Arnaud M., Piffaretti R., Böhringer H., Ponman T. J., Croston J. H., Voit G. M., Borgani S., Bower R. G., 2010, A&A, 511, 14
Rasia E., Tormen G., Moscardini L., 2004, MNRAS, 351, 237
Roychowdhury S., Ruszkowski M., Nath B. B., 2005, ApJ, 634, 90
Shaw L. D., Nagai D., Bhattacharya S., Lau E. T., 2010, ApJ, 725, 1452
Shi X., Komatsu E., Nelson K., Nagai D., 2015, MNRAS, 448, 1020
Simionescu A. et al., 2011, Science, 331, 1576
Soucail G., 2012, A&A, 540, 61
Springel V., Di Matteo T., Hernquist L., 2005, ApJ, 620, L79
Sunyaev R. A., Zeldovich Ya. B., 1972, Comments Astrophys. Space Sci., 4, 173
Sunyaev R. A., Zeldovich Ya. B., 1980, ARA&A, 18, 537
Su Y., Buote D., Gastaldello F., Brighenti F., 2015, ApJ, 805, 104
Tozzi P., Norman C., 2001, ApJ, 546, 63
Urban O. et al., 2014, MNRAS, 437, 3939
Valdarnini R., 2012, A&A, 546, A45
Vazza F., Brunetti G., Kritsuk A., Wagner R., Gheller C., Norman M., 2009, A&A, 504, 33
Vazza F., Dolag K., Ryu D., Brunetti G., Gheller C., Kang H., Pfrommer C., 2011, MNRAS, 418, 960
Vazza F., Eckert D., Simionescu A., Bröggen M., Ettori S., 2013, MNRAS, 429, 799
Vikhlinin A., Kravtsov A., Forman W., Jones C., Markevitch M., Murray S. S., Van Speybroeck L., 2006, ApJ, 640, 691
Vikhlinin A. et al., 2009, ApJ, 692, 1060
Voit G. M., Kay S. T., Bryan G. L., 2005, ApJ, 364, 909
Walker S. A. et al., 2013, MNRAS, 432, 554

APPENDIX A: SPH RESULTS

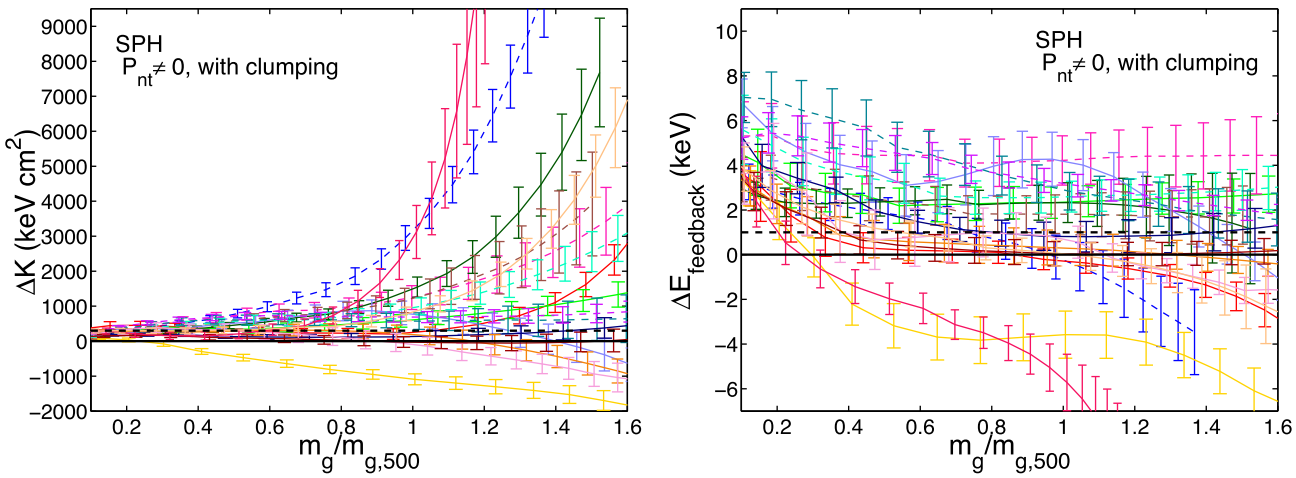

Figure A1. ΔK and ΔE profiles for SPH case.

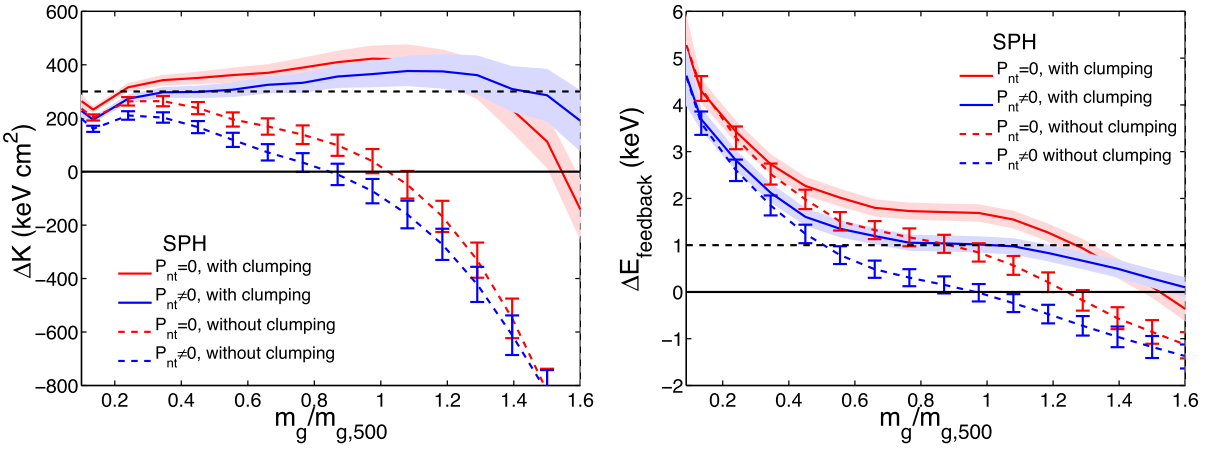

Figure A2. Comparison of ΔK and ΔE profiles for SPH case.

Table A1. Average feedback energy per particle $\epsilon_{\rm feedback}$ for SPH case with *Planck* $f_{\rm b} = 0.154$.

		Energy per particle (keV)					
		Without cooling energy			With cooling energy		
C	P_{nt}	$0.2–1r_{500}$	$0.2–1r_{200}$	$r_{500} - r_{200}$	$0.2–1r_{500}$	$0.2–1r_{200}$	$r_{500}–r_{200}$
				Full sample			
0	0	1.61 ± 0.21	0.86 ± 0.22	−0.25 ± 0.22	2.03 ± 0.21	1.13 ± 0.22	−0.19 ± 0.22
0	Nonzero	0.84 ± 0.20	0.19 ± 0.20	−0.79 ± 0.21	1.25 ± 0.20	0.46 ± 0.20	−0.73 ± 0.21
Nonzero	0	2.03 ± 0.20	1.59 ± 0.20	0.85 ± 0.20	2.41 ± 0.20	1.84 ± 0.20	0.90 ± 0.20
Nonzero	Nonzero	1.39 ± 0.19	1.10 ± 0.19	0.61 ± 0.18	1.77 ± 0.19	1.31 ± 0.19	0.62 ± 0.18
				NCC clusters			
0	0	0.95 ± 0.25	0.01 ± 0.26	−1.41 ± 0.28	1.37 ± 0.25	0.28 ± 0.26	−1.34 ± 0.28
0	Nonzero	0.18 ± 0.24	−0.64 ± 0.25	−1.89 ± 0.27	0.59 ± 0.25	−0.36 ± 0.25	−1.82 ± 0.26
Nonzero	0	1.38 ± 0.26	0.85 ± 0.28	−0.04 ± 0.30	1.76 ± 0.26	1.10 ± 0.28	0.01 ± 0.30
Nonzero	Nonzero	0.78 ± 0.25	0.42 ± 0.26	−0.15 ± 0.28	1.16 ± 0.25	0.68 ± 0.6	−0.10 ± 0.28
				CC clusters			
0	0	3.21 ± 0.41	2.57 ± 0.40	1.67 ± 0.36	3.62 ± 0.41	2.83 ± 0.40	1.72 ± 0.36
0	Nonzero	2.44 ± 0.39	1.85 ± 0.37	0.96 ± 0.34	2.85 ± 0.39	2.11 ± 0.37	1.01 ± 0.34
Nonzero	0	3.81 ± 0.44	3.50 ± 0.45	2.97 ± 0.48	4.18 ± 0.44	3.74 ± 0.45	3.01 ± 0.48
Nonzero	Nonzero	3.65 ± 0.45	3.25 ± 0.45	2.61 ± 0.44	4.05 ± 0.45	3.51 ± 0.45	2.66 ± 0.44

Table A2. Average feedback energy per particle $\epsilon_{\rm feedback}$ for SPH case with *WMAP* $f_{\rm b} = 0.167$.

		Energy per particle (keV)					
		Without cooling energy			With cooling energy		
C	P_{nt}	$0.2–1r_{500}$	$0.2–1r_{200}$	$r_{500}–r_{200}$	$0.2–1r_{500}$	$0.2–1r_{200}$	$r_{500}–r_{200}$
				Full sample			
0	0	2.02 ± 0.21	1.31 ± 0.22	0.23 ± 0.22	2.43 ± 0.21	1.58 ± 0.22	0.30 ± 0.22
0	Nonzero	1.25 ± 0.20	0.64 ± 0.20	−0.26 ± 0.20	1.67 ± 0.20	0.91 ± 0.20	−0.20 ± 0.20
Nonzero	0	2.38 ± 0.20	2.04 ± 0.20	1.49 ± 0.20	2.75 ± 0.20	2.30 ± 0.20	1.54 ± 0.20
Nonzero	Nonzero	1.72 ± 0.20	1.51 ± 0.19	1.17 ± 0.18	2.09 ± 0.20	1.73 ± 0.19	1.18 ± 0.18
				NCC clusters			
0	0	1.38 ± 0.25	0.49 ± 0.26	−0.86 ± 0.27	1.80 ± 0.25	0.77 ± 0.26	−0.79 ± 0.27
0	Nonzero	0.62 ± 0.24	−0.15 ± 0.25	−1.32 ± 0.25	1.04 ± 0.24	0.12 ± 0.25	−1.25 ± 0.25
Nonzero	0	1.74 ± 0.27	1.34 ± 0.28	0.69 ± 0.30	2.12 ± 0.27	1.60 ± 0.28	0.74 ± 0.30
Nonzero	Nonzero	1.12 ± 0.26	0.89 ± 0.26	0.50 ± 0.27	1.50 ± 0.26	1.15 ± 0.26	0.55 ± 0.27
				CC clusters			
0	0	3.63 ± 0.42	3.08 ± 0.41	2.27 ± 0.37	4.03 ± 0.42	3.34 ± 0.41	2.32 ± 0.37
0	Nonzero	2.87 ± 0.40	2.35 ± 0.38	1.63 ± 0.34	3.28 ± 0.40	2.61 ± 0.38	1.68 ± 0.34
Nonzero	0	4.14 ± 0.45	3.93 ± 0.46	3.56 ± 0.49	4.51 ± 0.45	4.17 ± 0.45	3.60 ± 0.49
Nonzero	Nonzero	4.04 ± 0.46	3.73 ± 0.46	3.26 ± 0.45	4.45 ± 0.46	4.00 ± 0.46	3.31 ± 0.45

This paper has been typeset from a TEX/LATEX file prepared by the author.